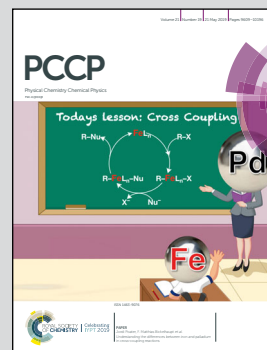


Showcasing research from the group of Prof. Jun Li at Chongqing University, China, and the group of Prof. Jörg Behler, Universität Göttingen, Germany.

A critical comparison of neural network potentials for molecular reaction dynamics with exact permutation symmetry

An accurate full-dimensional potential energy surface (PES) is key in molecular simulations. In this work, we compare the performance of four neural network-based approaches with rigorous permutation symmetry of like atoms for several typical reactions. The Jun group focuses on high-level PESes and reaction kinetics/dynamics. The Behler group focuses on the development and application of HD-NN potentials for a variety of systems from materials *via* gas-surface and solid-liquid interfaces to aqueous solutions.

As featured in:



See Jun Li, Jörg Behler et al., *Phys. Chem. Chem. Phys.*, 2019, 21, 9672.


 Cite this: *Phys. Chem. Chem. Phys.*,
2019, 21, 9672

A critical comparison of neural network potentials for molecular reaction dynamics with exact permutation symmetry

 Jun Li, *^{ab} Kaisheng Song^a and Jörg Behler *^b

The availability of accurate full-dimensional potential energy surfaces (PESs) is a mandatory condition for efficient computer simulations of molecular systems. Much effort has been devoted to developing reliable PESs with physically sound properties, such as the invariance of the energy with respect to the permutation of chemically identical atoms. In this work, we compare the performance of four neural network (NN)-based approaches with a rigorous permutation symmetry for fitting five typical reaction systems: OH + CO, H + H₂S, H + NH₃, H + CH₄ and OH + CH₄. The methods can be grouped into two categories, invariant polynomial based NNs and high-dimensional NN potentials (HD-NNPs). For the invariant polynomial based NNs, three types of polynomials, permutation invariant polynomials (PIPs), non-redundant PIPs (NRPIPs) and fundamental invariants (FIs), are used in the input layer of the NN. In HD-NNPs, the total energy is the sum of atomic contributions, each of which is given by an individual atomic NN with input vectors consisting of sets of atom-centered symmetry functions. Our results show that all methods exhibit a similar level of accuracy for the energies with respect to *ab initio* data obtained at the explicitly correlated coupled cluster level of theory (CCSD(T)-F12a). The HD-NNP method allows study of systems with larger numbers of atoms, making it more generally applicable than invariant polynomial based approaches, which in turn are computationally more efficient for smaller systems. To illustrate the applicability of the obtained potentials, quasi-classical trajectory calculations have been performed for the OH + CH₄ → H₂O + CH₃ reaction to reveal its complicated mode specificity.

 Received 7th November 2018,
Accepted 10th January 2019

DOI: 10.1039/c8cp06919k

rsc.li/pccp

1. Introduction

Within the Born–Oppenheimer realm, any reactive or non-reactive process can be considered to take place on an adiabatic potential energy surface (PES). Once the PES has been determined, various dynamical properties of the nuclei can be simulated according to either classical or quantum mechanical (QM) theory. Consequently, the performance of a simulation is largely determined by the accuracy of the underlying PESs. Therefore, developing accurate PESs is of great significance in the field of theoretical/computational chemistry. While the accuracy of empirical potentials relying on physical approximations is often limited, numerous approaches have been developed to represent PESs based on very flexible and purely mathematical functional forms, which can be grouped into two categories: (1) interpolation methods, which provide error-free energies

for the available reference data but interpolate in between, such as cubic splines, reproducing kernel Hilbert space (RKHS),¹ interpolating moving least square (IMLS)² and modified Shepard interpolation (MSI) methods;³ and (2) fitting methods relying on specific functional forms such as polynomials within the many body expansion regime,^{4,5} sum-of-product forms^{6,7} and permutation invariant polynomials (PIPs).^{8–10}

In spite of all these methods, the accurate description of global PESs has remained a formidable challenge even for comparably small polyatomic systems, because they often exhibit a complex topology with several reactants and products, saddle points and intermediates, and in general it is impossible to derive suitable functional forms based on physical considerations. A new promising class of PESs relies on machine learning (ML) techniques.^{11,12} While the first ML potentials employed artificial neural networks (NNs),^{13–15} in recent years many other methods have been proposed.^{12,16–18} NNs are “universal approximators”, as they are in principle able to approximate any unknown multidimensional function with arbitrary accuracy by “learning” from a large set of known function values.¹⁹ Recently, NNs have become a powerful tool to develop PESs for various systems with excellent fitting performance.^{14,15,20–27}

^a School of Chemistry and Chemical Engineering, Chongqing University, Chongqing 401331, China. E-mail: jli15@cqu.edu.cn

^b Universität Göttingen, Institut für Physikalische Chemie, Theoretische Chemie, Tammannstr. 6, 37077 Göttingen, Germany. E-mail: joerg.behler@uni-goettingen.de



One important property of any PES is that the potential energy values must be invariant under permutations of like atoms.^{28,29} Thus, a key issue is how to incorporate this permutation symmetry into PESs, which not only is important for constructing physically correct PESs, but also influences the efficiency of the sampling and the performance of the fitting process. For NN potentials, the first attempts to construct PESs with permutation symmetry have been made for electrolyte models of an ion interacting with fixed-geometry water monomers³⁰ and for molecule surface scattering employing frozen surfaces to reduce the dimensionality of the PES,^{20,31} but all these early attempts suffered from a very limited applicability.

The first NN potential with exact permutation symmetry for arbitrarily high-dimensional systems has been proposed by Behler and Parrinello in 2007.³² In these high-dimensional NN potentials (HD-NNPs), the total energy of the system is expressed as the sum of atomic energy contributions, which depend on the local atomic chemical environments that are described by many-body atom-centered symmetry functions.³³ For each element in the system there is a specific NN architecture with its associated weight parameters, making the resulting PES fully permutationally invariant.^{11,15,19,33–35} Although the method is based on atomic energy contributions, only total energies, not the individual atomic energies, are needed to optimize the parameters of NNs. The most important advantage of HD-NNPs is that this method is highly scalable for large systems of up to thousands of atoms with all their degrees of freedom considered explicitly. HD-NNPs have been constructed for a variety of mainly condensed systems with very different types of interactions from covalent bonds to metallic bonding and dispersion interactions.³⁵ In 2016, Guo and coworkers applied HD-NNPs to three prototypically reactive molecular systems, $H + H_2$, $H + H_2O$ and $H + CH_4$, with a Monte Carlo based method for efficiently selecting mapping functions. It should be noted that in their work, the points of the three systems have been sampled from pre-existing well-behaved analytical PESs, not from *ab initio* data sets.³⁶ In addition, Lu *et al.* employed the HD-NNP approach to fit the PES of the $H_2 + SH$ reaction based on *ab initio* calculated points, and the quantum dynamical results of the HD-NNP and PIP-NN PESs have been found to be essentially the same.³⁷

Building on the extensive work of Bowman and coworkers on molecular PESs based on permutation invariant polynomials (PIPs),^{10,29} in 2013, Guo and co-workers proposed to use PIPs in the input layer of a NN to obtain another type of NN potential with exact permutation invariance.^{24,25} In practice, all PIPs of Bowman and co-workers,^{8,9} truncated at a specified total degree, are used in the input layer of the NN. For a given system, the total degree of truncation is at least the highest degree of the primary and secondary invariants of the PIPs, and can be determined using Molien's series based on symmetry operations of the corresponding complete nuclear permutation and inversion (CNPI) group.^{38,39} If the degree is not sufficiently high, some primary or secondary invariants might be missing, and some additional "artificial" symmetry properties could be present in the PES. This approach is called PIP-NN, and combines the advantages of both the NN and PIP methods: the fitting performance is guaranteed

by the NN with rigorous permutation invariance incorporated by the PIPs.

However, the number of PIPs increases quickly with the number of degrees of freedom in the system. Therefore, it is hard to apply it directly to complicated systems, for instance, with more than approximately ten like atoms, as too many PIPs have to be used in the NN input layer. For instance, 1331 PIPs are used as the input layer of the NN for fitting the $OH + CH_4$ PES.⁴⁰ As many of the input PIPs are redundant, it is possible to express PIPs as functions of only the non-redundant terms corresponding to the primary and secondary invariant polynomials. Indeed, Xie and Bowman developed an algorithm to speed up the evaluation of the PIPs based on a straightforward symmetrization of a primitive monomial basis and the fact that any high-degree invariant polynomial constructed by using a monomial symmetrization approach can be decomposed into a product of two low-degree polynomials with a remainder invariant polynomial of the same degree.⁴¹ However, some redundant polynomials cannot be decomposed further by this approach for more complicated polyatomic systems. Nonetheless, one can use only the non-redundant terms of PIPs as the input layer of NNs for the fitting process. In 2016, for the $H + H_2S$ (A_3B) system, only 9 non-redundant PIPs have been used in the NN PES (NRPIP-NN), resulting in a root mean squared error (RMSE) of 6.9 meV, which is comparable to 3.9 meV by 4th-order PIPs (50 terms) and 3.0 meV by 3rd-order PIPs (22 terms), respectively.⁴² One can see that the number of the non-redundant terms is extremely small, especially for complicated systems.

Unfortunately, when the system becomes more complicated, the decomposition is hard to achieve completely. Consequently, some redundancy remains in the non-redundant PIPs, although redundancy is generally not a problem for NNs. It is known that all polynomials invariant under a given symmetry group can be represented as polynomials in a finite generating set of invariant polynomials, whose degree bound can also be determined. There exists a complete set of generating invariants for a given system, although their form is not unique. The complete set of the generating invariants for a given system can be determined according to King's algorithm, which has been implemented in software like MAGMA⁴³ and SINGULAR.⁴⁴ In 2013, Opalka and Domcke employed 31 generating invariant polynomials in their linear fitting of multi-sheeted PESs for A_4B molecules.⁴⁵ In 2016, Zhang and co-workers proposed to use the complete set of generating invariants of the system in the input layer of NNs.²⁷ Since generating invariants can generate all the invariant polynomials for a given symmetry group, they call them fundamental invariants (FIs) and the resulting fitting approach is called FI-NN. Because the number of the FIs increases mildly with the degree, as in the NRPIP mentioned above, the architecture of the FI-NN is more flexible resulting in a faster evaluation of the energy, in particular, for complicated systems, than for PIP-NNs.⁴⁶

All methods, PIP-NN, NRPIP-NN and FI-NN, employ invariant polynomials as the input layer of the NN. As systems become more and more complicated, it is harder and harder, and even impractical for high-dimensional systems beyond



approximately 10 like atoms, to employ these NN approaches due to the vast increase in the number of the polynomials, and it is difficult to determine the least order of the PIPs. In the HD-NNP method, on the other hand, such systems can directly be addressed with the same rigorous inclusion of the permutation invariance, although, with a few exceptions,^{46–51} to date it has been mainly applied to condensed systems.

In this work, the HD-NNP approach as implemented in the RuNNer code⁵² is examined for five prototypical reactions, OH + CO, H + H₂S, H + NH₃, H + CH₄ and OH + CH₄, whose PIP-NN PESs have been developed based on large numbers of high level *ab initio* data points.^{40,42,53–55} Note that to date HD-NNPs have been mainly applied to condensed systems with very high-dimensionality but a rather homogeneous spatial distribution of the atoms. On the other hand, for the reactive systems here, some inter-nuclear distances change within a large range while the number of atoms is rather small. NRPIP-NN and FI-NN approaches have been also examined and compared. The remainder of this publication is organized as follows. In section II, the relevant theory of the NN-based fitting methods is summarized. Then section III presents the comparison and discussion of these methods on fitting these five systems mentioned above. It has been shown that both PIP-NN PES and HD-NNP for the H + H₂S system yield essentially the same dynamical results by accurate quantum mechanical calculations. It is expected that the resulting different PESs of the same system should yield the same dynamical outcomes thanks to the high fidelity representation of the NN. As an application, the mode specificity in the OH + CH₄ reaction is studied by the quasi-classical trajectory (QCT) method based on the PIP-NN PES due to its much faster speed in evaluation, and relevant results and discussions are given in section IV. The conclusions and summary are presented in section V.

II. Theory

II-A. Invariant polynomial based NN

For constructing PESs, NNs serve as a non-linear fitting tool that converts signals, here the input vector $\mathbf{G} = \{G_i\}$ describing the atomic positions, to a scalar output E , the potential energy, via one or more hidden layers of the interconnected neurons. In most cases, a standard feed-forward NN with two hidden layers is sufficient for fitting PESs and its explicit form is,⁵⁶

$$E =$$

$$b_1^{(3)} + \sum_{k=1}^K \left(\omega_{1,k}^{(3)} \cdot f_2 \left(b_k^{(2)} + \sum_{j=1}^J \left(\omega_{k,j}^{(2)} \cdot f_1 \left(b_j^{(1)} + \sum_{i=1}^I \omega_{j,i}^{(1)} \cdot G_i \right) \right) \right) \right), \quad (1)$$

In eqn (1), I , J and K denote the size of the input layer, the neurons of the first and second hidden layers, respectively; f_i ($i = 1, 2$) are the transfer functions for the two hidden layers, for which we use a hyperbolic tangent in the present work; $\omega_{j,i}^{(l)}$ are weights that connect the i th neuron of a layer $l - 1$ and

the j th neuron of the layer l ; $b_j^{(l)}$ are biases of the j th neurons of the l th layer. The fitting parameters $\{\omega\}$ and $\{b\}$ are determined iteratively by minimizing the RMSE, as shown in eqn (2), as the performance function, typically employing gradient-based optimization algorithms.

$$\text{RMSE} = \sqrt{\sum_{i=1}^{N_{\text{data}}} \left(E_{\text{output}}^i - E_{\text{target}}^i \right)^2 / N_{\text{data}}}, \quad (2)$$

The input layer of the NN in general contains a set of functions of the atomic positions defining the molecular geometry. In the PIP-NN approach, PIPs of Morse-like variables of internuclear distances, R_{ij} , are used as the input layer of the NN: $\mathbf{G} = \hat{S} \prod_{i < j}^N p_{ij}^{l_{ij}}$, where $p_{ij} = \exp(-\alpha R_{ij})$, and \hat{S} is the symmetrization operator, which consists of all the permutation operations between atoms of the same element in the system.¹⁰ In practice, all PIPs up to a specific maximum order are included in the input layer. As discussed above, many PIPs are redundant. Therefore, we can also use only the non-redundant PIPs as the input layer, which can be determined in a straightforward fashion by the algorithm of Xie and Bowman.⁴¹ However, some redundancies might remain due to the possible incomplete decomposition of the algorithm in some practical systems. To overcome this possible problem, FI-NNs can be used with the input layer FIs containing only the smallest possible number of generating invariants.^{45,46}

For the PIP-NN, NRPIP-NN and FI-NN fitting methods, several different NN architectures with two or three hidden layers have been tested. For each architecture, 50–200 different NNs have been optimized differing in the initial randomly assigned fitting parameters. To avoid overfitting, the “early stopping” algorithm²¹ is used with the data divided randomly into three parts, *i.e.*, the training (90%), validation (5%) and test (5%) sets for each NN fitting. To minimize false extrapolation due to possible edge points in the randomly selected validation and test sets, only fits with similar RMSEs for all three sets are accepted as the final PES. Besides, the maximum deviation is a good criterion for choosing the final PIP-NN PES.

II-B. HD-NNPs

In the HD-NNP approach, the total energy E of a molecular system is expressed as the sum of atomic energy contributions E_i ,

$$E = \sum_{i=1}^{N_{\text{atom}}} E_i, \quad (3)$$

which depend on the local chemical environments of the atoms i up to a specified cutoff radius R_c . The E_i are given by individual atomic NNs, as shown in eqn (1), as a function of input vectors consisting of sets of many-body atom-centered symmetry function values, which serve as structural fingerprints to describe the geometric environments of the atoms within the cutoff-radius sphere. Several types of symmetry functions have



been proposed.³³ In this work, the following two types are used to describe the radial and angular interactions of the central atom i ,

$$G_{i,\text{tr}}^2 = \sum_j \exp(-\eta_{\text{tr}}(R_{ij} - R_{s,\text{tr}})^2) f_{c,\text{tr}}(R_{ij}), \quad (4)$$

$$G_{i,\text{ta}}^3 = 2^{1-\zeta_{\text{ta}}} \sum_{j < k, j, k \neq i} (1 + \lambda_{\text{ta}} \cos \theta_{ijk})^{\zeta_{\text{ta}}} \times \exp(-\eta_{\text{ta}}(R_{ij}^2 + R_{ik}^2 + R_{jk}^2)) \times f_{c,\text{ta}}(R_{ij}) f_{c,\text{ta}}(R_{ik}) f_{c,\text{ta}}(R_{jk}), \quad (5)$$

where the cut-off function is defined as,

$$f_c(R_{ij}) = \begin{cases} \left(\cos\left(\frac{\pi R_{ij}}{R_c}\right) + 1 \right) / 2 & \text{for } R_{ij} \leq R_c \\ 0 & \text{else} \end{cases} \quad (6)$$

In addition to the cut-off radius, R_c , which needs to be converged to include all energetically relevant atomic interactions, the parameters including R_s , λ , ζ and η defining the spatial shape of the symmetry functions have to be provided. The choice of the symmetry functions and the parameters is very important for the construction of HD-NNP PESs, as a reliable distinction of different structures is mandatory. To this end, several sets of parameters are used for the radial and angular interactions, and it is important to note that the symmetry functions are not simple two- and three-body terms but many-body functions that simultaneously depend on the positions of all atoms in the system. The subscripts “tr” and “ta” denote the t th or t ath of the radial and angular types of functions, respectively. The symmetry function sets can be determined empirically or systematically,^{36,57} and some discussion can be found in a previous investigation.¹⁹

In the invariant polynomial based NN approaches, the permutation symmetry is explicitly guaranteed by the symmetrization operators. It is worth presenting how the permutation symmetry is implemented in the HD-NNP approach explicitly. With A₂BC (like OH + CO) as an example, we label the atoms in the following order A(1)A(2)B(3)C(4). Then the components of the sum in eqn (4) and (5) read explicitly as,

$$G_{ij,\text{tr}}^2 = \exp(-\eta_{\text{tr}}(R_{ij} - R_{s,\text{tr}})^2) f_{c,\text{tr}}(R_{ij}), \quad (7)$$

$$G_{ijk,\text{ta}}^3 = 2^{1-\zeta_{\text{ta}}} (1 + \lambda_{\text{ta}} \cos \theta_{ijk})^{\zeta_{\text{ta}}} \exp(-\eta_{\text{ta}}(R_{ij}^2 + R_{ik}^2 + R_{jk}^2)) f_{c,\text{ta}}(R_{ij}) f_{c,\text{ta}}(R_{ik}) f_{c,\text{ta}}(R_{jk}), \quad (8)$$

For the central atom i being 1, 2, 3 and 4, the local chemical environments are described by the following functions:

$$G_{1,\text{t}} \begin{cases} G_{1,\text{tr}}^2 \begin{cases} = G_{12,\text{tr}}^2, & \text{AA} \\ = G_{13,\text{tr}}^2, & \text{AB} \\ = G_{14,\text{tr}}^2, & \text{AC} \end{cases} \\ G_{1,\text{ta}}^3 \begin{cases} = G_{123,\text{ta}}^3, & \text{AAB} \\ = G_{124,\text{ta}}^3, & \text{AAC} \\ = G_{134,\text{ta}}^3, & \text{ABC} \end{cases} \end{cases}, \quad (9)$$

$$G_{2,\text{t}} \begin{cases} G_{2,\text{tr}}^2 \begin{cases} = G_{21,\text{tr}}^2, & \text{AA} \\ = G_{23,\text{tr}}^2, & \text{AB} \\ = G_{24,\text{tr}}^2, & \text{AC} \end{cases} \\ G_{2,\text{ta}}^3 \begin{cases} = G_{213,\text{ta}}^3, & \text{AAB} \\ = G_{214,\text{ta}}^3, & \text{AAC} \\ = G_{234,\text{ta}}^3, & \text{ABC} \end{cases} \end{cases}, \quad (10)$$

$$G_{3,\text{t}} \begin{cases} G_{3,\text{tr}}^2 \begin{cases} = G_{31,\text{tr}}^2 + G_{32,\text{tr}}^2, & \text{BA} \\ = G_{34,\text{tr}}^2, & \text{BC} \end{cases} \\ G_{3,\text{ta}}^3 \begin{cases} = G_{312,\text{ta}}^3, & \text{BAA} \\ = G_{314,\text{ta}}^3 + G_{324,\text{ta}}^3, & \text{BAC} \end{cases} \end{cases}, \quad (11)$$

$$G_{4,\text{t}} \begin{cases} G_{4,\text{tr}}^2 \begin{cases} = G_{41,\text{tr}}^2 + G_{42,\text{tr}}^2, & \text{CA} \\ = G_{43,\text{tr}}^2, & \text{CB} \end{cases} \\ G_{4,\text{ta}}^3 \begin{cases} = G_{412,\text{ta}}^3, & \text{CAA} \\ = G_{413,\text{ta}}^3 + G_{423,\text{ta}}^3, & \text{CAB} \end{cases} \end{cases}, \quad (12)$$

As shown, for each central atom, the radial and the angular functions are grouped together according to their interaction types. If the central atom is A, there are three types of radial interactions, AA, AB and AC, and three types of angular interactions, AAB, AAC and ABC. For the central atom being B, there are only two types of radial interactions, BA and BC, and two types of angular interactions, BAA and BAC. The same situation holds for the central atom being C. According to eqn (3), the entire energy is expressed as follows:

$$E = \sum_{i=1}^{N_{\text{atom}}} E_i = NN_1(\{G_{1,\text{t}}\}) + NN_2(\{G_{2,\text{t}}\}) + NN_3(\{G_{3,\text{t}}\}) + NN_4(\{G_{4,\text{t}}\}), \quad (13)$$

Each NN_i corresponds to an equation like eqn (1) with the input variables $\{G_{i,\text{t}}\}$. The exchange of the two identical atoms 1 and 2 does not affect $\{G_{3,\text{t}}\}$ and $\{G_{4,\text{t}}\}$ at all, as shown in eqn (10) and (11). Therefore, NN_3 and NN_4 , which describe the environments of different elements, do not use the same NN: both the architectures and the fitting parameters of NN_3 and NN_4 are not restricted. On the other hand, the exchange of the two identical atoms 1 and 2 results in the permutation of the characterizations $\{G_{1,\text{t}}\}$ and $\{G_{2,\text{t}}\}$. Consequently, NN_1 and NN_2 must use the same NN: not only the architectures but also the fitting parameters of NN_1 and NN_2 are restricted to be the same. In this way, the entire energy is unchanged, as shown in eqn (14). In other words, the NN of each type of element in the system is restricted to be the same for the inclusion of the permutation symmetry property in the HD-NNP approach,



as has been stressed in ref. 11, 15, 19 and 33–35.

$$\begin{aligned}
 E &= \sum_{i=1}^{N_{\text{atom}}} E_i \\
 &= NN_1(\{G_{1,t}\}) + NN_1(\{G_{2,t}\}) + NN_3(\{G_{3,t}\}) + NN_4(\{G_{4,t}\}) \\
 &\stackrel{1 \leftrightarrow 2}{=} NN_A(\{G_{2,t}\}) + NN_A(\{G_{1,t}\}) + NN_B(\{G_{3,t}\}) + NN_C(\{G_{4,t}\}) \\
 &= \sum_j \sum_{i \in j} NN_i^j,
 \end{aligned} \tag{14}$$

It is also worth pointing out explicitly the significance of inclusion of the angular symmetry functions, eqn (5), for the correct description of the chemical environment of the central atom. If only radial symmetry functions are included, *i.e.*, only eqn (4) is used, eqn (9)–(12) would only have $G_{i,\text{tr}}^2$ ($i = 1-4$) left. One can easily find that the resulting fingerprints include additional “false symmetry” properties with respect to the permutations of the bond pair, either (r_{13}, r_{23}) or (r_{14}, r_{24}) , while the correct symmetry property for any A_2BC system is invariant with respect to the only permutation of two like atoms 1 and 2, which corresponds to two exchanges of (r_{13}, r_{23}) and (r_{14}, r_{24}) simultaneously. Hence, these radial symmetry functions $G_{i,\text{tr}}^2$ ($i = 1-4$) alone are insufficient to distinguish between these molecular configurations. Actually, similar situations have been pointed out and discussed in the PIP-NN approach.²⁵ Some additional cross terms, corresponding to the secondary invariants, have to be included to distinguish molecular configurations that have the same primary invariants.²⁸ The angular functions in the HD-NNP approach seem to function, to some extent, like the secondary invariants in the polynomial based NN approaches, PIP-NN, NRPP-NN and FI-NN.

III. Comparison of the fitting approaches

The five prototypical reactions $\text{OH} + \text{CO}$, $\text{H} + \text{H}_2\text{S}$, $\text{H} + \text{NH}_3$, $\text{H} + \text{CH}_4$ and $\text{OH} + \text{CH}_4$ have been studied extensively due to their fundamental significance in the field of quantum reaction dynamics. Full-dimensional accurate PESSs have been fitted with the PIP-NN approach for these systems based on large numbers of *ab initio* points calculated at the level of the explicitly correlated coupled cluster singles, doubles and perturbative triples with the augmented correlation corrected valence triple-zeta basis set (CCSD(T)-F12a/AVTZ).^{40,42,53–55} About 74 000, 34 000, 100 000, 63 000 and 135 000 points were calculated at the CCSD(T)-F12a/AVTZ level for the aforementioned systems, respectively. Their distributions are shown in Fig. 1–5(a). It can be seen that, most sampling points are of low to medium energies, albeit with some in the high energy regions, which is necessary for quantum dynamical calculations. First, the HD-NNP approach is used to fit these PESSs. For each system, different NN architectures with two or three hidden layers with different sets of atom-centered symmetry functions have

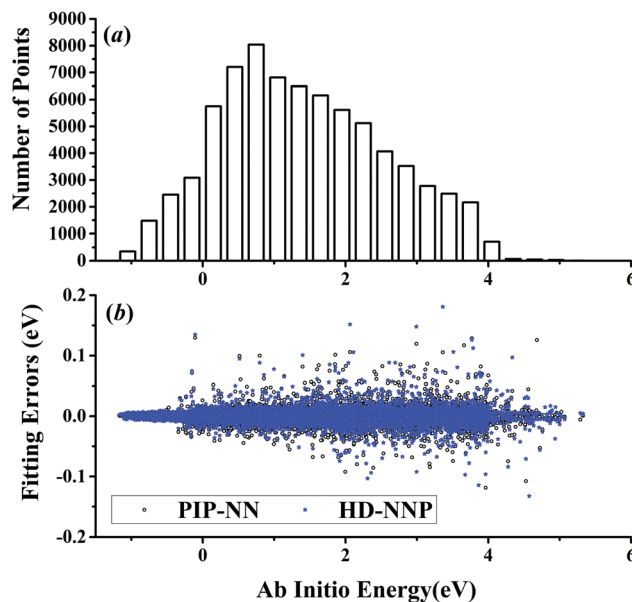


Fig. 1 (a) The distribution of the sampled points, and (b) PIP-NN and HD-NNP fitting errors (eV) as a function of the *ab initio* energy (eV) relative to the reactant asymptote for the $\text{OH} + \text{CO}$ system.

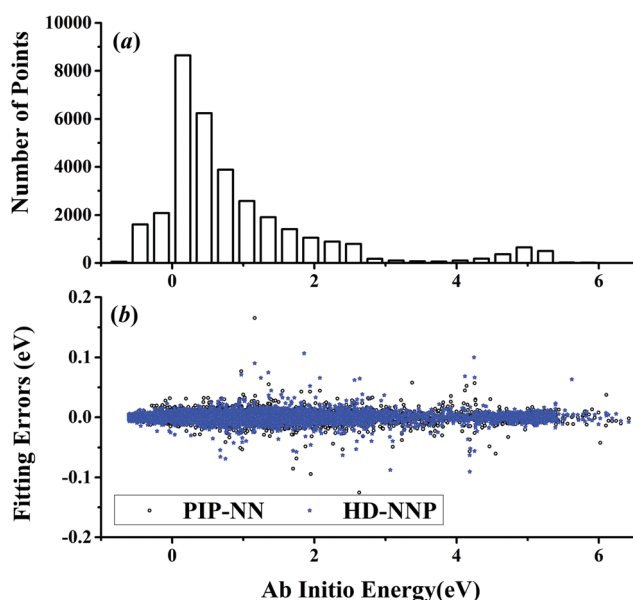
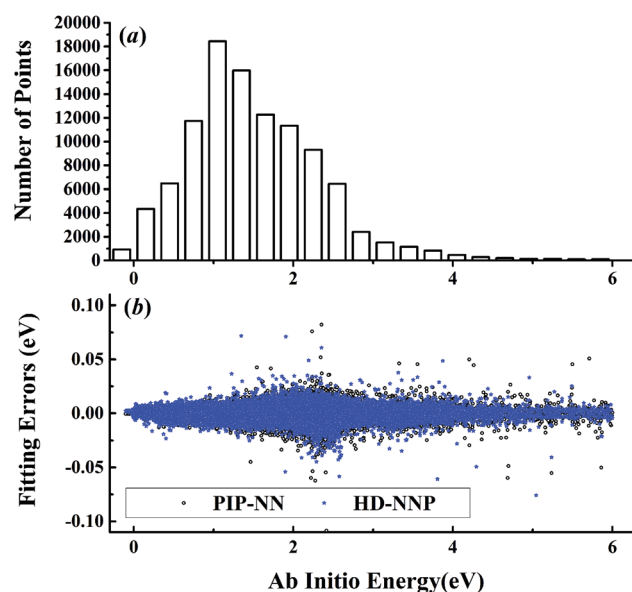
been carefully tested to identify the best fitting with its final total RMSE comparable to that by the PIP-NN approach. Although different NN architectures are in principle allowed for different elements in the HD-NNP approach, we found that using different numbers of layers or neurons per layer does not significantly improve the fitting performance. Hence, we choose to use the same NN architectures for all the elements in this work. Therefore, for each system, its entire NN structure can be specified as $n_A/n_B/n_C-n_1-n_2-1$: n_1 and n_2 denote the number of neurons in the first and second hidden layers, respectively; 1 corresponds to the output neuron, the energy; and $n_A/n_B/n_C$ are the number of atom-centered symmetry functions for elements A, B and C, constituting the input neurons. In this work, these systems are labeled as O_2CH , H_3S , H_4N , H_5C and H_5CO , respectively. Consequently, the number of the fitting parameters are given as $n_{\text{tA}}/n_{\text{tB}}/n_{\text{tC}}$ for elements A, B and C respectively. Table 1 shows the structures, number of fitting parameters (n_{tot}) and total RMSEs (meV) of the HD-NNP approach for these five systems above.

For $\text{OH} + \text{CO}$, the atomic environments of oxygen, carbon and hydrogen, have been described by 48, 32 and 32 atom-centered symmetry functions, respectively. Each of the two hidden layers possesses 60 neurons, resulting in 6661, 5701 and 5701 fitting parameters for oxygen, carbon and hydrogen, respectively. The total RMSE is 5.8 meV, compared to 5.5 meV of the total RMSE in the PIP-NN PES. However, the PIP-NN PES consists of only one NN, 17–50–80–1, with 5061 fitting parameters. Therefore, HD-NNP is slower than the PIP-NN PES. The HD-NNP RMSEs for H_3S , H_4N , H_5C and H_5CO are 5.0, 3.8, 8.0 and 4.7 meV, respectively, which are all comparable to those fitted by the PIP-NN approach, albeit with more fitting parameters. Unlike one NN used for the entire system in the



Table 1 Comparison of the structures, numbers of the fitting parameters (n_{tot}) and total RMSEs (meV) of the HO + CO, H + H₂S, H + NH₃, H + CH₄ and OH + CH₄ systems by the HD-NNP, PIP-NN, NRPIP-NN and FI-NN fitting methods

Systems	Items	HD-NNP	PIP-NN	NRPIP-NN	FI-NN
O ₂ CH	Structure	48/32/32–60–60–1	17–50–80–1	7–50–90–1	7–50–80–1
	n_{tot}	6661/5701/5701	5061	5081	4561
	RMSE	5.8	5.5	6.8	6.7
H ₃ S	Structure	28/14–20–80–1	22–20–60–1	9–40–50–1	9–30–60–1
	n_{tot}	2341/2061	1781	2501	2221
	RMSE	5.0	3.0	6.9	5.6
H ₄ N	Structure	28/14–60–60–1	81–20–80–1	38–30–70–1	31–30–60–1
	n_{tot}	5461/4621	3421	3411	2881
	RMSE	3.8	3.4	3.6	4.7
H ₅ C	Structure	28/14–60–60–1	848–4–100–1	203–15–45–1	
	n_{tot}	5461/4621	3997	3826	
	RMSE	8.0	5.1	6.3	
H ₅ CO	Structure	50/28/28–60–60–1	1331–4–100–1		
	n_{tot}	6781/5461/5461	5929		
	RMSE	4.7	3.9		

**Fig. 2** (a) The distribution of the sampled points, and (b) PIP-NN and HD-NNP fitting errors (eV) as a function of the *ab initio* energy (eV) relative to the reactant asymptote for the H + H₂S system.**Fig. 3** (a) The distribution of the sampled points, and (b) PIP-NN and HD-NNP fitting errors (eV) as a function of the *ab initio* energy (eV) relative to the reactant asymptote for the H + NH₃ system.

invariant polynomial based NN approaches, there are as many NNs as the number of atoms in HD-NNPs. Therefore, the HD-NNP is roughly the number of atoms slower in evaluation than the PIP-NN PES but more general. We note that in contrast to other HD-NNP applications reported in the literature, for which energy errors normalized per atom are given, the present RMSEs refer to energies of the entire system. Fig. 1–5(b) present the HD-NNP fitting errors along with the *ab initio* energy relative to the respective reactant asymptotes of the five systems. The PIP-NN fitting errors are also included for comparison. As shown clearly, both fitting approaches show similar fitting performance for these reactions: the small errors are evenly distributed within the energy range for each system. Therefore, the PESs from either the HD-NNP or PIP-NN are expected to give the same dynamical results, as has been demonstrated for the reaction H₂ + HS.³⁷ Furthermore, Fig. 6 presents the comparison of the contour plots

of the HD-NNP and PIP-NN PESs along the two reaction coordinates, r_{OH} and r_{CH} , for the abstraction reaction OH + CH₄ → H₂O + CH₃. They are essentially identical. In the inset of the same figure, the minimum energy paths of the PIP-NN and HD-NNP PESs and by the *ab initio* calculation are also indistinguishable from each other, confirming the equivalence of the two fitting approaches.

NRPIP-NN and FI-NN are then compared by fitting PESs for OH + CO, H + H₂S and H + NH₃, whose FIs are available.⁴⁶ As has been mentioned above, the form of the invariant polynomials is not unique. Taking A₂B, A(1)A(2)B(3), as an example, FIs and NRPIPs are given explicitly in Table 2. For A₂B systems, NRPIPs are essentially the same as FIs, as $G_3 = (f_2^2 - f_3)/2$. However, the evaluation of G_3 is faster than that of f_3 due to more evaluations of the polynomials involved in f_3 . Similar situations hold for A₂BC and A₃B: the evaluation of



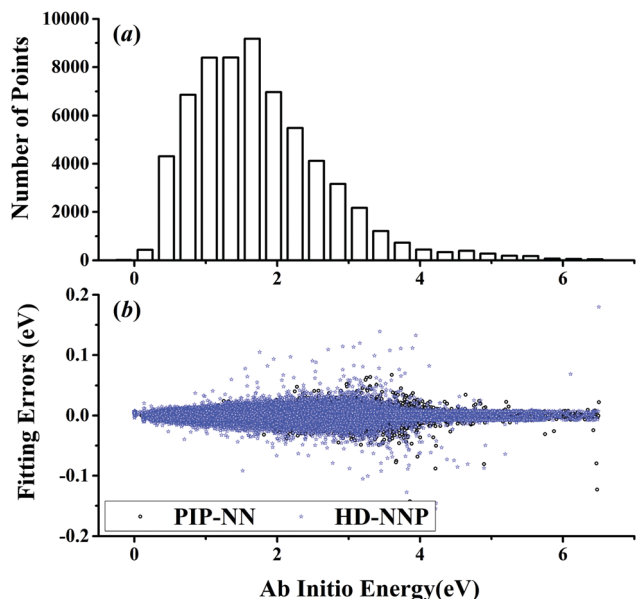


Fig. 4 (a) The distribution of the sampled points, and (b) PIP-NN and HD-NNP fitting errors (eV) as a function of the *ab initio* energy (eV) relative to the reactant asymptote for the H + CH₄ system.

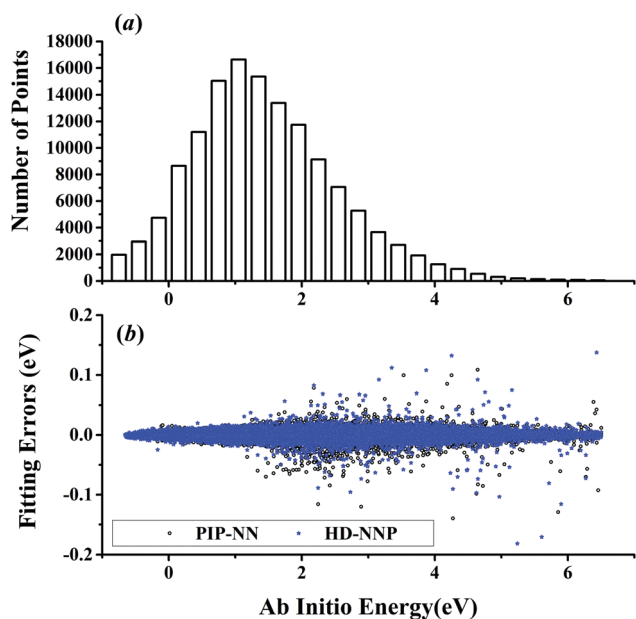


Fig. 5 (a) The distribution of the sampled points, and (b) PIP-NN and HD-NNP fitting errors (eV) as a function of the *ab initio* energy (eV) relative to the reactant asymptote for the OH + CH₄ system.

NRPIPs is 10% faster than that of FIs, as shown also in Table 2. Indeed, for O₂CH and H₃S, NRPIPs and FIs are essentially the same as each other, as they can be converted to each other with the same number of terms. For NH₄, the number of NRPIPs is larger than that of FIs due to the incomplete decomposition of the algorithm. Nonetheless, the resulting fitting errors of the OH + CO, H + H₂S and H + NH₃ systems with the two fitting approaches resemble each other, as shown in Fig. 7(a–c).

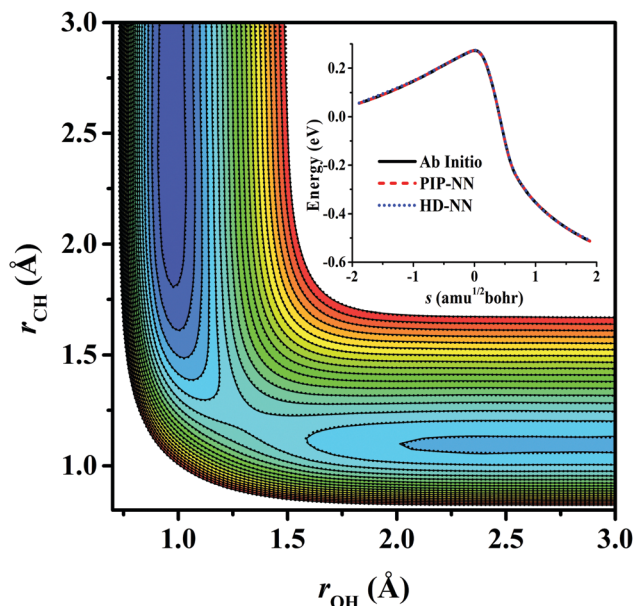


Fig. 6 Contour plots of the OH + CH₄ → H₂O + CH₃ reaction along the two reactive coordinates, r_{OH} and r_{CH} (in Å) on the PIP-NN (solid line) and HD-NNP (dotted line) PESs. The other coordinates are fixed at the transition state. The energies are in eV relative to the reactant asymptote. The comparison of the minimum energy path on the PIP-NN and HD-NNP PESs and by the *ab initio* calculation is also shown in the inset.

As shown in Table 1, the percentages of the FIs or NRPIPs become smaller with the molecular size: for O₂CH and H₃S, it is 7/17 and 9/22 for both methods; for H + NH₃, it is 35/81 for NRPIP-NN and 31/81 for FI-NN. Finally, the H + CH₄ system is fitted by the NRPIP-NN approach, resulting in a total RMSE of 6.3 meV with 203 NRPIPs from 848 PIPs. One can see that for complicated systems, the number of the NRPIPs is still quite large. The fitting errors in Fig. 7(d) resemble those by PIP-NN and HD-NN, as shown in Fig. 4.

IV. Mode specificity of OH + CH₄

Mode specificity is defined by the differences in reactivity due to excitations in various reactant modes. It is an important and interesting non-statistical phenomenon in reaction dynamics, and related to the laser control of reactions. In this work, the mode specificity in the vibrational modes of the reactants for the OH (ν_{OH}) + CH₄ (ν_{u} , ν_{rock} , ν_{ss} , ν_{as}) → H₂O + CH₃ reaction is studied by the QCT implemented in the VENUS chemical dynamics program.⁵⁸ There are four types of vibrational modes in the CH₄ reactant, namely, umbrella, rock, symmetric stretch and asymmetric stretch modes. The HD-NNP and PIP-NN PESs are expected to yield the same dynamical results, as has been demonstrated in our previous work.^{36,37} However, the PIP-NN PES is much faster with relatively smaller RMSEs. Therefore, the PIP-NN PES is used in the subsequent computations. At the collision energies of 4.0, 10.0, 15.0, 20.0, 25.0 and 30.0 kcal mol^{−1} (1 eV = 23.06 kcal mol^{−1}), 7–15 × 10⁴ trajectories are calculated with initial reactants being at the ro-vibrational ground states



Table 2 Comparison of NRPIPs and FIs for A₂B, A₂BC and A₃B systems

	NRPIPs	FIs
A ₂ B	$\begin{cases} G_1 = x_{12} \\ G_2 = x_{13} + x_{23} \\ G_3 = x_{13}x_{23} \end{cases}$	$\begin{cases} f_1 = x_{12} \\ f_2 = x_{13} + x_{23} \\ f_3 = x_{13}^2 + x_{23}^2 \end{cases}$
A ₂ BC	$\begin{cases} G_1 = x_{13} + x_{23} \\ G_2 = x_{14} + x_{24} \\ G_3 = x_{13}x_{23} \\ G_4 = x_{14}x_{24} \\ G_5 = x_{13}x_{24} + x_{14}x_{23} \\ G_6 = x_{12} \\ G_7 = x_{34} \end{cases}$	$\begin{cases} f_1 = x_{13} + x_{23} \\ f_2 = x_{14} + x_{24} \\ f_3 = x_{13}^2 + x_{23}^2 \\ f_4 = x_{14}^2 + x_{24}^2 \\ f_5 = x_{13}x_{14} + x_{23}x_{24} \\ f_6 = x_{12} \\ f_7 = x_{34} \end{cases}$
A ₃ B	$\begin{cases} G_1 = x_{12} + x_{13} + x_{23} \\ G_2 = x_{14} + x_{24} + x_{34} \\ G_3 = x_{34}x_{13} + x_{34}x_{14} + x_{24}x_{14} \\ G_4 = x_{14}x_{23} + x_{24}x_{13} + x_{34}x_{12} \\ G_5 = x_{23}x_{13} + x_{23}x_{12} + x_{13}x_{12} \\ G_6 = x_{12}x_{13}x_{23} \\ G_7 = x_{34}x_{14}x_{23} + x_{24}x_{14}x_{23} + x_{34}x_{24}x_{12} \\ \quad + x_{14}x_{24}x_{13} + x_{24}x_{34}x_{12} + x_{14}x_{34}x_{12} \\ G_8 = x_{24}x_{23}x_{13} + x_{14}x_{23}x_{13} + x_{34}x_{23}x_{12} \\ \quad + x_{14}x_{23}x_{12} + x_{34}x_{13}x_{12} + x_{24}x_{13}x_{12} \\ G_9 = x_{14}x_{24}x_{34} \end{cases}$	$\begin{cases} f_1 = x_{12} + x_{13} + x_{23} \\ f_2 = x_{14} + x_{24} + x_{34} \\ f_3 = x_{12}^2 + x_{13}^2 + x_{23}^2 \\ f_4 = x_{14}^2 + x_{24}^2 + x_{34}^2 \\ f_5 = x_{12}x_{14} + x_{13}x_{14} + x_{13}x_{34} \\ \quad + x_{23}x_{34} + x_{23}x_{24} + x_{12}x_{24} \\ f_6 = x_{12}^3 + x_{13}^3 + x_{23}^3 \\ f_7 = x_{14}^3 + x_{24}^3 + x_{34}^3 \\ f_8 = x_{12}^2x_{14} + x_{13}^2x_{14} + x_{13}^2x_{34} \\ \quad + x_{23}^2x_{34} + x_{23}^2x_{24} + x_{12}^2x_{24} \\ f_9 = x_{14}^2x_{23} + x_{34}^2x_{12} + x_{24}^2x_{13} \end{cases}$

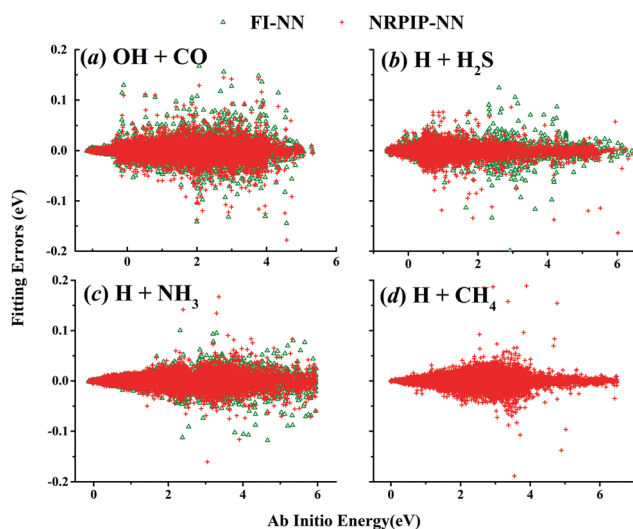


Fig. 7 NRPIP-NN and FI-NN fitting errors (eV) as a function of the *ab initio* energy (eV) relative to the reactant asymptote for OH + CO (a), H + H₂S (b) and H + NH₃ (c), respectively, and NRPIP-NN fitting errors (eV) for H + CH₄ (d).

($v = 0$), or with one vibrational mode excited by one quantum ($v = 1$). For each different initial condition, the maximum impact parameter (b_{\max}) is determined using small batches of trajectories with trial values. Then the impact parameter b for each trajectory is sampled according to $b = b_{\max} \text{RN}^{1/2}$, where RN is a random number between 0 and 1. The initial separation

between the reactants and the termination criteria for non-reactive and reactive processes are both set as 8.0 Å. The scattering parameters including the spatial orientation of the initial reactants, vibrational phases and the impact parameter, are determined according to the Monte Carlo approach as implemented in VENUS.⁵⁸ The propagation time step is selected to be 0.05 fs and the gradients of the PES with respect to atomic coordinates are calculated numerically. The combined fourth-order Runge–Kutta and sixth-order Adams–Moulton algorithms are used for the integration of the trajectories. Almost all trajectories conserve energy within a chosen criterion (10^{-4} kcal mol⁻¹). The reactive integral cross section (ICS) is calculated according to the following formula:

$$\sigma_r(E_c) = \pi b_{\max}^2(E_c) P_r(E_c), \quad (15)$$

where the reaction probability $P_r(E_c)$ at the specified collision energy E_c is given by the ratio between the number of reactive trajectories (N_r) and the total number of trajectories (N_{total}): $P_r(E_c) = N_r/N_{\text{total}}$ with the standard error given by $\Delta = \sqrt{(N_{\text{total}} - N_r)/N_{\text{total}}N_r}$. In this work, the statistical errors are all less than 4.0% except for $E_c = 4.0$ kcal mol⁻¹, at which the statistical error is less than 8%.

Fig. 8(a) presents the corresponding ICSs along the collision energy. At the ground state ($v = 0$) of the reactants, the reactivity at 4.0 kcal mol⁻¹ is very small, which is consistent with the zero point energy (ZPE) corrected barrier height of 4.6 kcal mol⁻¹.⁴⁰ Then the reactive ICS increases monotonically with the collision energy,



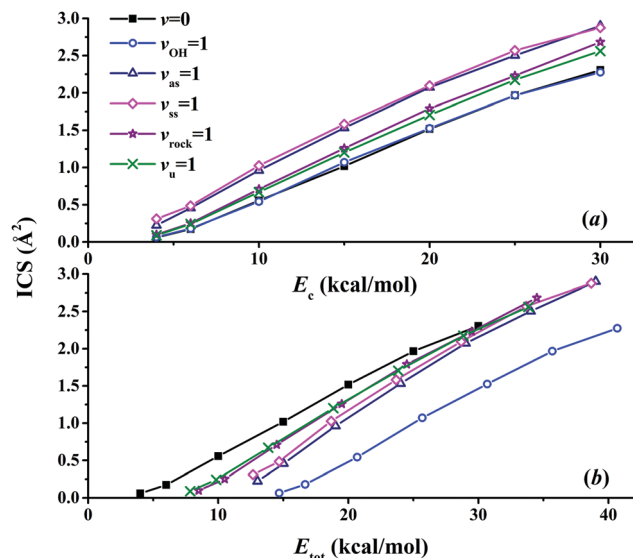


Fig. 8 The calculated integral cross sections (ICSs) for the OH (ν_{OH}) + CH₄ (ν_{u} , ν_{rock} , ν_{ss} , ν_{as}) \rightarrow H₂O + CH₃ reaction as a function of (a) the collision energy and (b) the total energy.

which is common for activated reactions. When one of the vibrational modes in the reactants is excited by one quantum, all the resulting ICSs still go up monotonically with the collision energy. However, their effects on the reactivity are different. In order to see their effects clearly and directly, scaled ICSs are defined as $\text{ICS}(\nu_i = 1, E_c) / \text{ICS}(\nu = 0, E_c)$, and are plotted in Fig. 9. As shown clearly, the OH vibrational mode is essentially a spectator within the range of the collision energy, as expected since OH is not involved in the bond forming or breaking during the chemical reaction. On the other hand, all the vibrational modes of the CH₄ reactant enhance the reaction significantly, especially at low collision energy. For instance, at $E_c = 4 \text{ kcal mol}^{-1}$, the scaled ICSs are 3.74, 5.22, 1.65 and 1.49, for $\nu_{\text{as}} = 1$, $\nu_{\text{ss}} = 1$, $\nu_{\text{rock}} = 1$ and $\nu_{\text{u}} = 1$, respectively. At this low collision energy, their effects are significantly different. Along with the collision energy, initially, the scaled ICSs of all the vibrational modes of the CH₄ reactant drop down drastically, then decrease gradually, and finally tend to become flat eventually. Besides, the effects of the symmetric and asymmetric stretching modes are always larger, compared to the umbrella and rock modes within the energy range. At $E_c = 30 \text{ kcal mol}^{-1}$, the scaled ICSs read 1.26, 1.25, 1.16 and 1.11, for $\nu_{\text{as}} = 1$, $\nu_{\text{ss}} = 1$, $\nu_{\text{rock}} = 1$ and $\nu_{\text{u}} = 1$, respectively. The promoting effect by the excitation of the C–H stretch mode was also found in the $\text{OH} + \text{CHD}_3 \rightarrow \text{H}_2\text{O} + \text{CD}_3$ reaction by reduced-dimensional quantum dynamical (QD) and full-dimensional QCT calculations.⁵⁹ However, the excitation of the umbrella mode was found to be a spectator in that work.⁵⁹

In order to compare the relative efficacies of the reactant modes and the collision energy in promoting the reaction, the ICSs are also plotted in Fig. 8(b) as a function of the total energy, which is defined as the sum of the initial ro-vibrational energy relative to the ZPE corrected reactant asymptote and the collision energy. As shown clearly, all the energy thresholds are

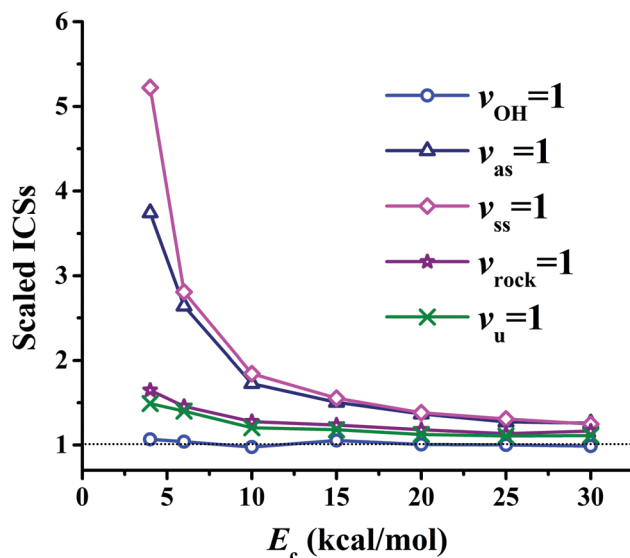


Fig. 9 The scaled ICSs for the OH (ν_{OH}) + CH₄ (ν_{u} , ν_{rock} , ν_{ss} , ν_{as}) \rightarrow H₂O + CH₃ reaction as a function of the collision energy.

shifted to higher energies for the reactants in the vibrationally excited states ($\nu = 1$), indicating that not all vibrational energies are used to surmount the potential barrier. The efficacy of the OH vibrational mode is never higher than the collision energy due to its spectator nature. For vibrational modes of the CH₄ reactant, the situation is complicated. With the total energy up to *ca.* 30 kcal mol^{-1} , the collision energy is more effective in promoting the reaction than all vibrational modes of CH₄. This is consistent with the prediction according to the Polanyi rules for this early-barrier reaction. With even higher total energy, it seems that the efficacies of all the vibrational modes of CH₄ become comparable to that of the collision energy. On the other hand, the different efficacies of the vibrational modes cannot be explained simply. These findings are also significantly different from those in the $\text{OH} + \text{CHD}_3 \rightarrow \text{H}_2\text{O} + \text{CD}_3$ reaction: the reactivity was found to be largely enhanced by the excitation of the C–H stretch mode at high total energies larger than *ca.* 14 kcal mol^{-1} .⁵⁹

Based on the assumption of the sudden approximation, namely, the intramolecular vibrational relaxation (IVR) of the reactants is much slower than the collision time scale, the recently proposed sudden vector projection model (SVP) attributes the efficacy of the specified reactant mode in promoting the reaction to its coupling with the reaction coordinate at the transition state.^{60–63} In particular, it is quantified approximately by the overlap between the reactant normal mode vector and the reaction coordinate vector. For the OH + CH₄ reaction, the calculated SVP values are 0.31, 0.42, 0.02, 0.09, 0.01 and 0.43, respectively, for the asymmetric stretch, symmetric stretch, rock and umbrella modes of CH₄, the OH vibrational mode and the collision motion.⁶² The spectator nature of the OH vibrational mode is consistent with the near-zero SVP value. On the other hand, SVP predicts that symmetric and asymmetric stretch modes are much more effective than the rock and umbrella modes in promoting the reactivity. In addition, the rock and umbrella

modes should have small efficacies. The collision motion is the most effective in promoting the reaction compared to the vibrational modes of the reactants. However, Fig. 8(b) shows that: at low total energies, the rock and umbrella modes are more effective than the stretch modes, and the efficacies of all the vibrational modes of CH₄ become similar to each other along with the total energy eventually. Although the QCT results resemble the QD results for activated reactions generally, one should bear in mind that QCT cannot describe QM effects, such as ZPE conservation, tunneling and resonance. Besides, the time scale of IVR might be comparable to that of the collision time for complicated molecular systems. Therefore, it is highly desirable to perform accurate QM calculations, albeit too demanding for the 15-dimensional system currently. Nonetheless, the complicated mode specificity of this reaction dynamics cannot be understood in a simple way.

We note in passing that several investigations have been reported on the SVP model in predicting the mode specificity of H/F/Cl + CH₄/CHD₃ reactions.^{59,62,64–67} The SVP predictions are generally in good agreement with QCT or QD computations. For instance, in the H + CHD₃ → H₂ + CD₃ reaction, it has been found that all excitations in the C–H stretch, and the CD₃ umbrella motions enhance the reactivity significantly with the collision energy of up to 36.9 kcal mol^{−1},⁶⁸ consistent with the SVP values, 0.98 and 0.21.⁶² However, the SVP value for the CH bending motion is 0.0, in contradiction to the evident enhancement at high total energies calculated by QD.⁶⁸ In the F + CHD₃ reaction, the C–H stretch excitation enhances the reactivity for the product channel HF + CD₃, and has no effect on the other product channel DF + CHD₂. These QCT calculations are consistent with the SVP values: 0.14 and 0.01.⁶⁵ However, the SVP model may not be appropriate due to the existence of the pre-reaction well for this reaction with a low barrier height, as pointed out earlier.⁶² In Cl + CHD₃ → HCl + CD₃ reaction, the C–H stretch excitation was found to promote the reactivity significantly,⁶⁹ consistent again with the large SVP value: 0.93.⁶² Interested readers are also referred to those references for further detailed discussions on the SVP predictions.

V. Conclusions

Recently, fitting global PESs for molecular systems with NNs has attracted much attention, primarily due to its efficiency and high fidelity. Any PES must be invariant with respect to nuclear permutation and the inversion group. This is not only because the molecular Hamiltonian commutes with the symmetry operators of the system, but also because a PES without permutation and inversion symmetries might yield false spectroscopic and reaction dynamics outcomes. In this study, several different symmetry strategies in the NN approach, including HD-NNP, PIP-NN, NRPIP-NN and FI-NN, have been compared in fitting several prototypical reaction systems, OH + CO, H + H₂S, H + NH₃, H + CH₄ and OH + CH₄. For each NN, it takes several hours to days to get the optimal fitting. The fitting results demonstrate that the three invariant polynomial based approaches

are effectively equivalent, consistently exhibiting similar energy errors in representing the five reaction systems. The form of the invariant polynomials is not unique and the comparison between NRPIP and FI shows that evaluation of NRPIPs is faster than that of FIs.

For very high dimensional systems with several tens and even up to thousands of atoms, it is impractical to determine their invariant polynomials. This issue is addressed by the HD-NNP, which also include full permutation invariance and in which the total energy is expressed as the sum of atomic contributions. HD-NNP is highly scalable, and has been applied successfully in fitting various practical systems. In this work, it is found that the HD-NNP works well in fitting the small systems mentioned above, but typically relies on more fitting parameters.

The mode specificity of the OH + CH₄ → H₂O + CH₃ reaction has been studied using the QCT approach on the globally accurate PIP-NN PES. It has been found that resulting mode specificity is rather complicated. All the vibrational modes of CH₄ can enhance the reaction, especially at low collision energies. The OH mode is essentially a spectator. Compared to the collision energy, all the vibrational modes of CH₄ are less effective in promoting the reaction with total energies less than *ca.* 30 kcal mol^{−1}. This is consistent with the prediction according to the Polanyi rules for this early barrier reaction. For the total energies larger than 30 kcal mol^{−1}, the efficacies of the CH₄ vibrational modes are comparable to that of the collision energy. The results are partially consistent with the SVP predictions for the stretching modes, the collision motion, and the OH vibrational mode, while the efficacies of the low frequency modes, rock and umbrella modes of CH₄, are underestimated significantly by the SVP model. Both the intrinsic flaw of QCT and the possible slow IVR in the complicated CH₄ system could be the cause to yield such results.

Conflicts of interest

There are no conflicts of interest to declare.

Acknowledgements

This work was financially supported by National Natural Science Foundation of China (Contract No. 21573027 to J. L.) and by the Alexander von Humboldt Foundation (Humboldt Fellowship for Experienced Researchers for JL). JB acknowledges the DFG for a Heisenberg Professorship (Be3264/11-2).

References

- 1 T. Hollebeek, T.-S. Ho and H. Rabitz, *Annu. Rev. Phys. Chem.*, 1999, **50**, 537–570.
- 2 M. Majumder, S. A. Ndengue and R. Dawes, *Mol. Phys.*, 2016, **114**, 1–18.
- 3 M. A. Collins, *Theor. Chem. Acc.*, 2002, **108**, 313–324.



- 4 J. N. Murrell, S. Carter, S. C. Farantos, P. Huxley and A. J. C. Varandas, *Molecular Potential Energy Functions*, Wiley, Chichester, 1984.
- 5 A. J. C. Varandas, *Adv. Chem. Phys.*, 1988, **74**, 255–338.
- 6 A. Jackle and H.-D. Meyer, *J. Chem. Phys.*, 1996, **104**, 7974.
- 7 A. Jackle and H.-D. Meyer, *J. Chem. Phys.*, 1998, **109**, 3772.
- 8 B. J. Braams and J. M. Bowman, *Int. Rev. Phys. Chem.*, 2009, **28**, 577–606.
- 9 J. M. Bowman, G. Czako and B. Fu, *Phys. Chem. Chem. Phys.*, 2011, **13**, 8094–8111.
- 10 C. Qu, Q. Yu and J. M. Bowman, *Annu. Rev. Phys. Chem.*, 2018, **69**, 151–175.
- 11 J. Behler, *J. Chem. Phys.*, 2016, **145**, 170901.
- 12 V. Botu, R. Batra, J. Chapman and R. Ramprasad, *J. Phys. Chem. C*, 2017, **121**, 511–522.
- 13 T. B. Blank, S. D. Brown, A. W. Calhoun and D. J. Doren, *J. Chem. Phys.*, 1995, **103**, 4129–4137.
- 14 C. M. Handley and P. L. A. Popelier, *J. Phys. Chem. A*, 2010, **114**, 3371–3383.
- 15 J. Behler, *Phys. Chem. Chem. Phys.*, 2011, **13**, 17930–17955.
- 16 A. P. Bartók, M. C. Payne, R. Kondor and G. Csányi, *Phys. Rev. Lett.*, 2010, **104**, 136403.
- 17 M. Rupp, A. Tkatchenko, K.-R. Müller and O. A. von Lilienfeld, *Phys. Rev. Lett.*, 2012, **108**, 058301.
- 18 E. V. Podryabinkin and A. V. Shapeev, *Comput. Mater. Sci.*, 2017, **140**, 171–180.
- 19 J. Behler, *Int. J. Quantum Chem.*, 2015, **115**, 1032–1050.
- 20 S. Lorenz, A. Groß and M. Scheffler, *Chem. Phys. Lett.*, 2004, **395**, 210–215.
- 21 L. M. Raff, R. Komanduri, M. Hagan and S. T. S. Bukkapatnam, *Neural Networks in Chemical Reaction Dynamics*, Oxford University Press, Oxford, 2012.
- 22 J. Chen, X. Xu, X. Xu and D. H. Zhang, *J. Chem. Phys.*, 2013, **138**, 221104.
- 23 J. Chen, X. Xu and D. H. Zhang, *J. Chem. Phys.*, 2013, **138**, 154301.
- 24 B. Jiang and H. Guo, *J. Chem. Phys.*, 2013, **139**, 054112.
- 25 J. Li, B. Jiang and H. Guo, *J. Chem. Phys.*, 2013, **139**, 204103.
- 26 S. Manzhos, R. Dawes and T. Carrington, *Int. J. Quantum Chem.*, 2015, **115**, 1012–1020.
- 27 K. Shao, J. Chen, Z. Zhao and D. H. Zhang, *J. Chem. Phys.*, 2016, **145**, 071101.
- 28 J. Ischtwan and M. A. Collins, *J. Chem. Phys.*, 1991, **94**, 7084–7097.
- 29 A. Brown, B. J. Braams, K. Christoffel, Z. Jin and J. M. Bowman, *J. Chem. Phys.*, 2003, **119**, 8790–8793.
- 30 H. Gassner, M. Probst, A. Lauenstein and K. Hermansson, *J. Phys. Chem. A*, 1998, **102**, 4596–4605.
- 31 J. Behler, S. Lorenz and K. Reuter, *J. Chem. Phys.*, 2007, **127**, 014705.
- 32 J. Behler and M. Parrinello, *Phys. Rev. Lett.*, 2007, **98**, 146401.
- 33 J. Behler, *J. Chem. Phys.*, 2011, **134**, 074106.
- 34 J. Behler, *J. Phys.: Condens. Matter*, 2014, **26**, 183001.
- 35 J. Behler, *Angew. Chem., Int. Ed.*, 2017, **56**, 12828–12840.
- 36 B. Kolb, B. Zhao, J. Li, B. Jiang and H. Guo, *J. Chem. Phys.*, 2016, **144**, 224103.
- 37 D. Lu, J. Qi, M. Yang, J. Behler, H. Song and J. Li, *Phys. Chem. Chem. Phys.*, 2016, **18**, 29113–29121.
- 38 J. Ischtwan and M. A. Collins, *J. Chem. Phys.*, 1994, **100**, 8080–8088.
- 39 A. Schmelzer and J. N. Murrell, *Int. J. Quantum Chem.*, 1985, **28**, 287–295.
- 40 J. Li and H. Guo, *J. Chem. Phys.*, 2015, **143**, 221103.
- 41 Z. Xie and J. M. Bowman, *J. Chem. Theory Comput.*, 2010, **6**, 26–34.
- 42 D. Lu and J. Li, *J. Chem. Phys.*, 2016, **145**, 014303.
- 43 W. Bosma, J. Cannon and C. Playoust, *J. Symb. Comput.*, 1997, **24**, 235–265.
- 44 G.-M. Greuel, G. Pfister and H. Schönemann, SINGULAR 3.0.4—A computer algebra system for polynomial computations, 2007, see <http://www.singular.uni-kl.de>.
- 45 D. Opalka and W. Domcke, *J. Chem. Phys.*, 2013, **138**, 224103.
- 46 B. Fu and D. H. Zhang, *J. Chem. Theory Comput.*, 2018, **14**, 2289–2303.
- 47 K. V. J. Jose, N. Artrith and J. Behler, *J. Chem. Phys.*, 2012, **136**, 194111.
- 48 M. Gastegger and P. Marquetand, *J. Chem. Theory Comput.*, 2015, **11**, 2187–2198.
- 49 M. Gastegger, C. Kauffmann, J. Behler and P. Marquetand, *J. Chem. Phys.*, 2016, **144**, 194110.
- 50 B. Jiang, J. Li and H. Guo, *Int. Rev. Phys. Chem.*, 2016, **35**, 479–506.
- 51 J. S. Smith, O. Isayev and A. E. Roitberg, *Chem. Sci.*, 2017, **8**, 3192–3203.
- 52 J. Behler, *RunNer-A code for constructing high-dimensional neural network potentials*, Georg-August-Universität, 2018.
- 53 J. Li, J. Chen, D. H. Zhang and H. Guo, *J. Chem. Phys.*, 2014, **140**, 044327.
- 54 J. Li and H. Guo, *Phys. Chem. Chem. Phys.*, 2014, **16**, 6753–6763.
- 55 J. Li, J. Chen, Z. Zhao, D. Xie, D. H. Zhang and H. Guo, *J. Chem. Phys.*, 2015, **142**, 204302.
- 56 C. M. Bishop, *Neural Networks for Pattern Recognition*, Oxford University Press, Inc., New York, NY, USA, 1995, ISBN:0198538642.
- 57 G. Imbalzano, A. Anelli, D. Giofré, S. Klees, J. Behler and M. Ceriotti, *J. Chem. Phys.*, 2018, **148**, 241730.
- 58 X. Hu, W. L. Hase and T. Pirraglia, *J. Comput. Chem.*, 1991, **12**, 1014–1024.
- 59 H. Song, Y. Lu, J. Li, M. Yang and H. Guo, *J. Chem. Phys.*, 2016, **144**, 164303.
- 60 B. Jiang and H. Guo, *J. Chem. Phys.*, 2013, **138**, 234104.
- 61 B. Jiang and H. Guo, *J. Am. Chem. Soc.*, 2013, **135**, 15251–15256.
- 62 B. Jiang and H. Guo, *J. Chin. Chem. Soc.*, 2014, **61**, 841–959.
- 63 H. Guo and B. Jiang, *Acc. Chem. Res.*, 2014, **47**, 3679–3685.
- 64 R. Welsch and U. Manthe, *J. Chem. Phys.*, 2014, **141**, 051102.
- 65 C. Xie, B. Jiang, M. Yang and H. Guo, *J. Phys. Chem. A*, 2016, **120**, 6521–6528.
- 66 R. Ellerbrock and U. Manthe, *J. Chem. Phys.*, 2017, **147**, 241104.
- 67 R. Ellerbrock and U. Manthe, *J. Chem. Phys.*, 2018, **148**, 224303.
- 68 Z. Zhang, J. Chen, S. Liu and D. H. Zhang, *J. Chem. Phys.*, 2014, **140**, 224304.
- 69 Z. Zhang, Y. Zhou, D. H. Zhang, G. Czako and J. M. Bowman, *J. Phys. Chem. Lett.*, 2012, **3**, 3416–3419.

